Earth Planets Space, **59**, 1149–1153, 2007

Feasibility study on the potential of satellite altimetry for detecting seismic geoid changes due to the 2004 Sumatra-Andaman earthquake

Yutaka Hayashi[1], Kenji Hirata[1], Tsurane Kuragano[2], Toshiyuki Sakurai[3], Hiromi Takayama[1], Yohei Hasegawa[4], and Nobuo Hamada[4]

[1]*Seismology and Volcanology Research Department, Meteorological Research Institute, Nagamine 1-1, Tsukuba 305-0052, Japan*
[2]*Global Environment and Marine Department, Japan Meteorological Agency, Otemachi 1-3-4, Chiyoda-ku, Tokyo 100-8122, Japan*
[3]*Office of Planning, Meteorological Research Institute, Nagamine 1-1, Tsukuba 305-0052, Japan*
[4]*Seismological and Volcanological Department, Japan Meteorological Agency, Otemachi 1-3-4, Chiyoda-ku, Tokyo 100-8122, Japan*

(Received July 22, 2005; Revised September 14, 2007; Accepted October 2, 2007; Online published November 30, 2007)

Sea surface height data obtained by satellite altimetry from Jason-1 and TOPEX/Poseidon were analyzed to explore the possibility of a seismic geoid change due to the 2004 Sumatra-Andaman earthquake. This analysis identified a weakly positive geoid change in a region between the trench and outer arc. A subsequent investigation of the characteristics of this coseismic geoid change based on the dislocation theory revealed that a positive peak should indicate the upper edge of the high-slipped area or asperity and that a negative peak is responsible for the lower edge of the earthquake fault. An attempt at modeling the difference in the sea level anomaly failed to explain the observation since a large scatter in the original dataset obstructed its confirmation.
Key words: Asperity, coseismic geoid change, Jason-1, satellite altimetry, sea surface height, TOPEX/Poseidon, 2004 Sumatra-Andaman earthquake.

1. Introduction

The 2004 Sumatra-Andaman earthquake that caused the tsunami in the Indian Ocean on December 26 was the largest seismic event worldwide in 40 years. It was a multi-segmented earthquake along the Sunda trench subduction zone (McCloskey *et al*., 2005), and the seismic fault extends for 1300 km (Ishii *et al*., 2005). Standard seismological approaches are insufficient for gathering precise knowledge on the main shock due to some slow slip on a time scale beyond the seismographical band in the northern part of the fault (Ammon *et al*., 2005).

Although a coseismic geoid change has never been observed, geoid change analysis using satellite altimetry data seems to be a possible non-seismic approach for unraveling the mechanisms of huge earthquakes with slow slip beyond the seismographical frequency band. In general, the geoid is approximately equal to the average sea surface height. A change in geoid, therefore, would be approximately equal to the average change in the sea surface height (SSH). Okubo (1994) predicted that a coseismic geoid change caused by an earthquake of magnitude 9 could possibly be detected by satellite altimetry through the change in SSH because such a geoid change would theoretically be expected to reach the order of centimeters (Sun and Okubo, 1998). Using roughly assumed fault parameters, Sabadini *et al*. (2005) calculated that the expected geoid change caused by the 2004 Sumatra-Andaman earthquake is approximately 1.8 cm peak-to-peak. A detailed distribution of the coseismic geoid change enable scientists to determine the seismic fault model precisely (Okubo, 1994). If profiles of coseismic geoid changes across the trench were to be obtained, the distribution of asperities could be described. The profiles parallel to the trench would provide information on the extent of the fault zone.

If the 2004 Sumatra-Andaman earthquake caused coseismic geoid change, permanent displacements of the order of centimeters on average SSH could be produced. These would affect the monitoring of oceanographic phenomena, such as sea currents in the northeastern Indian Ocean. If this were the case, the geoid change or changes in SSH could be used as correction values for oceanographic monitoring.

In the study reported here, we examined the potential of using satellite altimetry data to detect coseismic geoid changes caused by the 2004 Sumatra-Andaman earthquake.

2. Methods

2.1 Data

Satellite altimetry measures the distance from the satellite to the sea surface using a microwave radar (Fig. 1) to monitor global oceanographic phenomena and map the Earth's gravity field. Altimeters are carried on board satellites whose tracks can be controlled and analyzed with highly accurate references.

2.1.1 Altimeters We used observation data obtained from altimeters (C- and Ku-band microwave radars) on board TOPEX/Poseidon and its successor, Jason-1. Both satellites were on 10-day cycles operated by the U.S. National Aeronautics and Space Administration (NASA) and the Centre National D'etudes Spatiales, France (CNES).

NASA routinely processes observed SSHs to eliminate

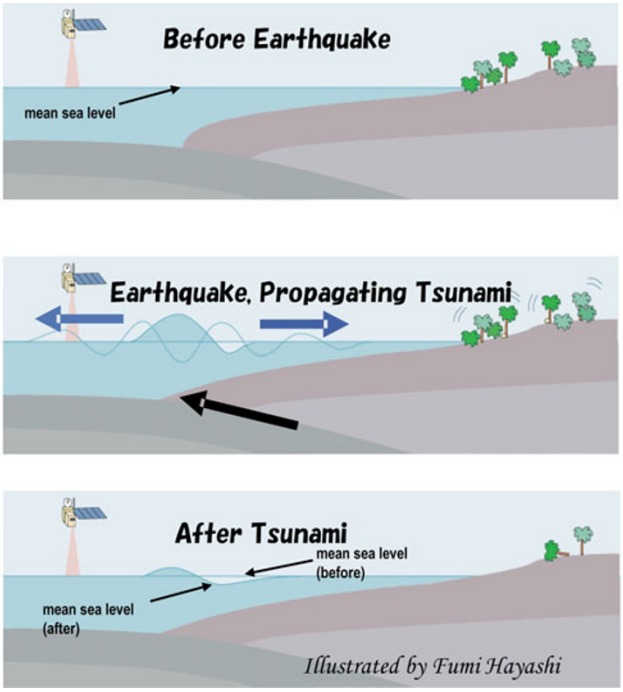

Fig. 1. An ocean tsunami and a coseismic geoid change caused by a huge earthquake may be observed by satellite altimetry. Satellite altimetry observes the distance from the satellite to the sea surface just below. Averaged SSHs, which are almost equal to geoid heights, change because of the disturbed gravity field by the redistribution of mass caused by huge earthquakes. Satellites with altimeters in favorable tracks and schedules may observe ocean tsunamis in propagation and, as such, they may also observe coseismic geoid changes.

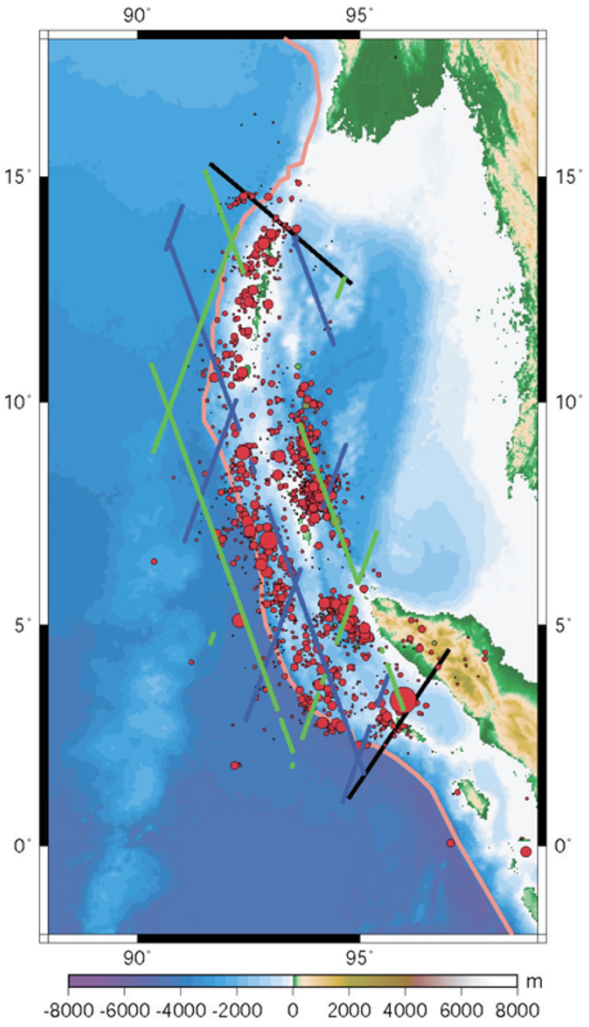

Fig. 2. Area for analysis of the changes in SLA before and after the 2004 Sumatra-Andaman earthquake. The curved pink line indicates the Sunda trench identified by Bird (2003). The target area to be analyzed is between the two black lines. Blue lines indicate the distribution of the sampling points on six tracks of Jason-1, and green lines indicate the five tracks of TOPEX/Poseidon. Solid circles plot the epicenters of the main shock and the aftershocks ($M \geq 4.0$) through February 16, 2005, as identified by National Earthquake Information Center, U.S. Geological Survey (2005). We used ETOPO2, based on the work of Smith and Sandwell (1997), by National Geophysical Data Center, National Oceanic and Atmospheric Administration of U.S. (NGDC, NOAA) for elevation and bathymetry data.

the effects of geoid locality, ocean tides, air pressure, and atmospheric vapor. The sea level anomalies (SLAs) obtained after the data processing are open to users through the Physical Oceanography Distributed Active Archive Center, Jet Propulsion Laboratory (PO.DAAC/JPL). Sea level anomalies consist of the total effects of sea currents, seawater temperature, surface winds, and other oceanographical phenomena, including observation errors. According to the fact sheets (NASA, 2001a, b), the accuracies of the SLAs are 4.2 cm and less than 4.2 cm for TOPEX/Poseidon and Jason-1, respectively.

2.1.2 Period We used SLA products provided by PO.DAAC/JPL and NASA for the period from November 4, 2004 to February 16, 2005, with the exception of data on December 26, 2004 due to the tsunami caused by the 2004 Sumatra-Andaman earthquake (Gower, 2005). We divided the entire data period into two time frames: (1) November 4 to December 25, 2004 and (2) December 27, 2004 to February 16, 2005. Each of these two time frames included five cycles of both TOPEX/Poseidon and Jason-1.

2.1.3 Area We defined the survey area as shown in Fig. 2. The eastern edge of the area is 300 km east of the Sunda trench and the western edge is 150 km to its west. The area is approximately 1300 km long along the Sunda trench. This length equals that of aftershock area determined by National Earthquake Information Center, U.S. Geological Survey (NEIC/USGS) up to February 16, 2005.

2.2 Data processing

2.2.1 Resampling We divided SLA data into bins at latitude intervals of 0.05 degrees along every track-segment of both satellites. We first selected the bins that included three or more observations; from these, we then selected those bins with one or more observations in each time frame, as defined in Section 2.1.2. The total number of bins thus selected was 312, of which 67 originated from TOPEX/Poseidon and 245 from Jason-1. Figure 2 depicts the locations of the available selected bins.

2.2.2 Estimation of background levels Although oceanographic phenomena show temporal and spatial variation, we assumed that seasonal variation is small within months. We defined the background level (BGL) at the i-th

sampling bin ($i = 1, 2, \ldots, 312$) as

$$\mathrm{BGL}_i \equiv 0.6745\sigma_{\mathrm{SLA}_i} \tag{1}$$

where σ_{SLA_i} is the standard deviation of the SLA data in the i-th sampling bin during the observation period mentioned in 2.1.2. In other words, the BGL_i is the difference between the average SLA_i and its quartile determined under the assumption that SLA data follows a normal distribution. If σ_{SLA_i} defined by Eq. (1) is smaller than the accuracies described in 2.1.1, the expected observation error from the typical accuracy (2.5 cm) of SLA products is used instead of σ_{SLA_i} in order to avoid an underestimation of the BGL.

2.2.3 Calculation of change of the SLA We defined the difference in the SLA at the i-th sampling bin between two time frames as

$$\mathrm{dSLA}_i \equiv \overline{\mathrm{SLA}_{i,\mathrm{after}}} - \overline{\mathrm{SLA}_{i,\mathrm{before}}} \tag{2}$$

where $\overline{\mathrm{SLA}_{i,\mathrm{before}}}$ and $\overline{\mathrm{SLA}_{i,\mathrm{after}}}$ are the average SLA at i-th sampling bin for five satellite-cycled periods before the main shock (November 4 to December 25, 2004) and after that (December 27, 2004 to February 16, 2005), respectively.

2.2.4 Relationship between the distance and change of the SLA We calculated the averaged dSLA every 10 km in the distance range of -150 km to $+300$ km measured perpendicular to the trench. The sign of the distance refers to the location of the observation points with respect to the trench (negative, west; positive, east). We defined these as

$$\mathrm{dSLA}_{x\,\mathrm{km}} \equiv \sum_{\text{for all } i} w_i \,\mathrm{dSLA}_i \tag{3}$$

$$w_i = \mathrm{BGL}_i{}^{-2} \Big/ \sum_{\text{for all } i} \mathrm{BGL}_i{}^{-2} \tag{4}$$

where w_i is the weight for the i-th sampling bin, which is centered at x in the distance range within the range from $x-10$ km to $x+10$ km. For example, $\mathrm{dSLA}_{+50\,\mathrm{km}}$ indicates the weighted average of change of the SLA at all sampling bins between $+40$ km and $+60$ km from the trench.

We evaluated the estimation errors in determining $\mathrm{dSLA}_{x\,\mathrm{km}}$ from the BGLs at each sampling bin in the area using the error transfer theory as

$$\mathrm{ERR}_{x\,\mathrm{km}} = \sqrt{\sum_{\text{for all } i} w_i \cdot \mathrm{BGL}_i{}^2} \tag{5}$$

where $\mathrm{ERR}_{x\,\mathrm{km}}$ is the averaged background level at x km from the trench.

3. Results

Figure 3 shows the differences in the average SLA for five satellite-cycle intervals before and after the 2004 Sumatra-Andaman earthquake; the difference between these values is on the order of centimeters at the very most. This figure shows a large scatter in the original SLA distribution (small blue and green dots in Fig. 3). The large scatter masks the identification of a possible coseismic geoid change due to the 2004 Sumatra-Andaman earthquake. There are many distinct local peaks and troughs in the dSLA distribution.

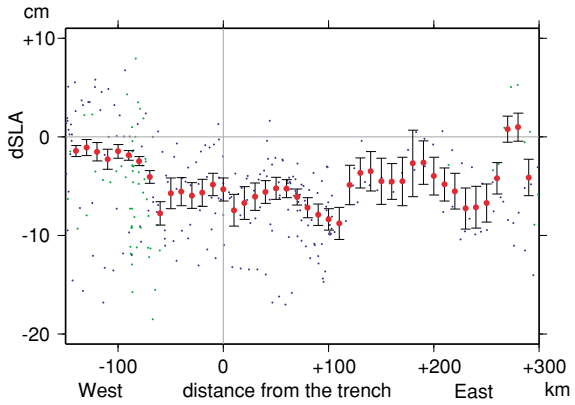

Fig. 3. Change in SLA before and after the 2004 Sumatra-Andaman earthquake. Signs of the distance refer to where the sampling points are located in relation to the trench (negative, west; positive, east). The dSLA is defined as the difference in averaged SLA before (November 4 to December 25, 2004) and after (December 27, 2004 to February 16, 2005) the main shock (Eq. (2)). Small blue dots indicate the sampling points on the track of Jason-1, and green dots indicate those of TOPEX/Poseidon. Large red dots with error bars indicate averaged dSLAs in a 20-km width (Eq. (3)) and background levels (Eq. (5)). For example, the dSLA at $+100$ km is defined as the average of dSLA for all sampling points falling within an area 100 ± 10 km east of the Sunda trench.

There is a positive peak (-5.2 ± 1.1 cm) 50 km east of the trench and a negative one (-8.8 ± 1.6 cm) 110 km to the east. The resulting crest-to-trough change in SLA before and after the main shock is 4 ± 2 cm. The following parameters are included in this value: effects by non-seismic oceanographic phenomena, post-seismic effects, and inaccuracies caused by the satellite altimeters.

4. Discussion

4.1 Theoretical coseismic geoid change

Sun and Okubo (1998) used the dislocation theory to establish equations representing coseismic geoid change by a finite fault. Figure 4 presents some examples of our calculations using their equations in which we assumed four cases. The first one is "case 0," which is defined by a uniform slip of 14 m, with a width of 150 km, and a length of 1300 km (Hirata *et al.*, 2006). We modified "case 0" to prepare the other three cases, allowing heterogeneous slip in the dip direction. We divide fault plane into three sections in the dip direction (Fig. 4(c)). "Case U" has a high-slipped area in the top third of the fault plane; "case M" has a high-slipped area in the middle third; "case B" has the high-slipped area in the bottom third. In all of these cases, the total seismic moment is fixed to 3.5×10^{10} N m (approx. $M_{\mathrm{w}} = 9.3$).

The theoretical coseismic geoid changes calculated from the four cases above shows the following characteristics.

(1) The geoid change perpendicular to the trench was more significant than that parallel to it (Fig. 4(a)).
(2) One positive peak and one negative peak was found in the geoid change profile perpendicular to the trench (Fig. 4(b)).
(3) The positive peak of the geoid change profile perpendicular to the trench was almost above the upper

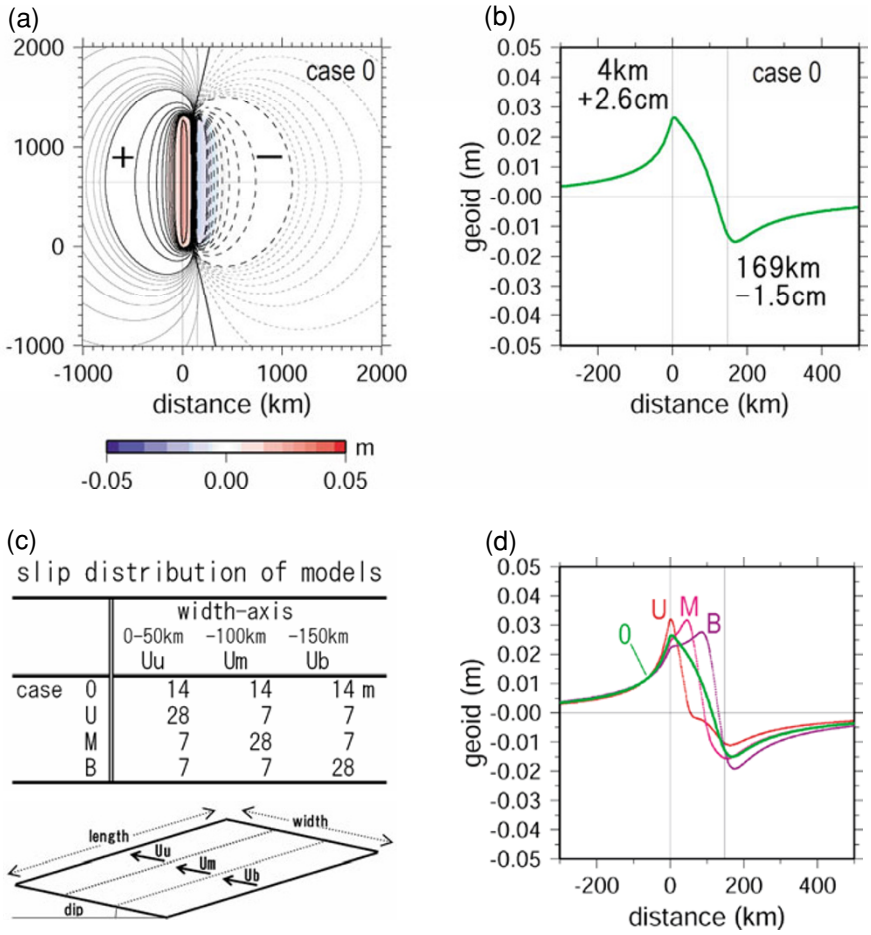

Fig. 4. Calculated coseismic geoid change caused by a long shallow low-angled reverse fault models equivalent to an $M_w = 9.3$ earthquake. (a) Distribution of the coseismic geoid change by "case 0" was calculated using the dislocation theory (Sun and Okubo, 1998). The original point in the top left box indicates the location of one of the up-dip corners of the fault. (b) The cross section of calculated coseismic geoid change by "case 0", along the line parallel to the x-axis passes through the center of the fault. (c) Four models on slip distribution. The moments of assumed fault slips are equivalent to $M_w = 9.3$ with an assumed rigidity of 3.5×10^{10} N/m^2. Model parameters are as follows: length, 1300 km; width, 150 km; depth of the upper edge, 10 km; dip, 10 degrees; average slip, 14 m; slip distribution, as shown at the bottom left; rake, 90 degrees; density of crust, 2.67×10^3 kg/m^3. (d) Comparison of the cross sections of calculated coseismic geoid change for each model shown in (c), along the line parallel to the x-axis, passing through the center of the fault.

edge of the high-slipped area; the negative peak was almost above the lower edge of the earthquake fault (Fig. 4(d)).

(4) The crest-to-trough geoid change reached several centimeters.

(5) Absolute geoid change larger than a centimeter was limited in the region between approximately 100 km seaward from the upper edge of the earthquake fault and 150 km landward from the lower edge of it (Fig. 4(d)).

4.2 Interpretation of results

According to Ammon *et al.* (2005), the slip of the 2004 Sumatra-Andaman earthquake was likely confined within the region extending from the trench to approximately 200 km to the east. In this case, a possible coseismic geoid change may have contributed to the observed SLA change between +50 km and +110 km shown in Fig. 3, similar to the model geoid change pattern (Section 4.1, points (1), (2), and (3); Fig. 4). The observed crest-to-trough value (4 ± 2 cm) was consistent with possible coseismic geoid changes calculated from equivalent cases with $M_w = 9.3$ (case 0, 4.2 cm; case M, 4.7 cm). Observed positive peak locations (50 km east of the trench) possibly indicated the approximate location of the upper edge of a possible high-slipped area of the earthquake fault of the main shock, based on the characteristics of coseismic geoid changes discussed in Section 4.1, point (3). However, large errors with observed SLA change lying more than +100 km to the east and a step between +110 km and +120 km of unknown cause suggest that the negative peak location is not well determined.

As shown in Fig. 3, we were also able to identify three other SLA changes greater than the BGLs that were also similar to model geoid change patterns characterized in Section 4.1 points (1), (2), and (4). These were located between −100 km and −60 km (peak-to-peak: 6 ± 1 cm), between +110 km and +140 km (peak-to-peak: 5 ± 3 cm), and between +280 km and +290 km (peak-to-peak: 5 ± 2 cm). If these patterns involved non-seismic noises, similar noises could possibly affect the observed peak-to-peak change (4 ± 2 cm) of the SLA both before and after the main shock as well as the peak locations (+50 km and +110 km).

Although we also calculated the SLA change pattern in our provisional previous study (Hayashi *et al.*, 2006), the results of this paper depend on a more reliable data processing, as described in Section 2.2.

4.3 Improving methodology

One approach to reducing the noise levels further would be to reanalyze sea surface height data obtained by satellite altimetry from both the Jason-1 and TOPEX/Poseidon satellites over a longer time interval. If the SLA differences were to be analyzed for periods longer than 1 year both before and after the main shock, we would at the very least expect a reduction of noise, including seasonal oceanographic phenomena.

Mass redistribution caused by an earthquake affects both gravity potential fields and absolute changes in gravity. Coseismic gravity changes caused by the 2004 Sumatra-Andaman earthquake were detected through the gravity mission of NASA's GRACE (Gravity Recovery and Climate Experiment) satellites (Han *et al.*, 2006). GRACE satellites observe gravity at 300–500 km above sea level, far from a seismic source. On the other hand, Jason-1's altimeters observe sea surface, whose average resembles geoids and where there are only several tens of kilometers above a typical inter-plate earthquake fault. If SSH data for longer time periods from satellite altimetry do contribute to a reduction in seasonal noise, the estimate of the two-dimensional distribution of seismic geoid change would possible be brought into better resolution in comparison to the observations by the GRACE satellite.

5. Conclusions

We analyzed sea surface height (SSH) data obtained from satellite altimetry of Jason-1 and TOPEX/Poseidon and found that the geoid, which was approximately equal to the average SSH, was possibly changed coseismically from a few to several centimeters in peak-to-peak by the 2004 Sumatra-Andaman earthquake.

Theoretical consideration based on the dislocation model suggested that the upper edge location of a high-slipped area or an asperity determined the location of the maximum in coseismic geoid change and that the lower edge of the entire earthquake fault plane coincides with the minimum. The observed temporal difference of the average SLA may indicate that such a maximum and minimum are located approximately 50 km and 110 km, respectively, east of the Sunda trench. However, a great deal of scatter in the differences of the SLA before and after the earthquake obstructed a clear identification of the peak and trough.

To confirm our results, we should reanalyze SSH data from satellite altimetry over a longer period and compare these with other geodetic findings on the 2004 Sumatra-Andaman earthquake.

Acknowledgments. We are grateful to two anonymous reviewers for their valuable comments. We are also grateful to Ms. F. Hayashi for drawing the concept illustration (Fig. 1). We prepared some figures (Figs. 2–4) using the Generic Mapping Tools (Wessel and Smith, 1999). PO.DAAC, JPL, NASA provided the satellite altimetry data from Jason-1 and TOPEX/Poseidon. This work was partially supported by the Special Coordination Funds for Promoting Science and Technology, from Ministry of Education, Sports, Culture, Science and Technology of Japan (MEXT).

References

Ammon, C. J., C. Ji, H. Thio, D. Robinson, S. Ni, V. Hjorleifsdottir, H. Kanamori, T. Lay, S. Das, D. Helmberger, G. Ichinose, J. Polet, and D. Wald, Rupture process of the 2004 Sumatra-Andaman earthquake, *Science*, **308**, 1133–1139, 2005.

Bird, P., An updated digital model of plate boundaries, *Geochem. Geophys. Geosyst.*, **4**, 1027, doi:10.1029/2001GC00252, 2003.

Gower, J., Jason 1 Detects the 26 December 2004 Tsunami, *EOS Trans. AGU*, **86**, 37–38, 2005.

Han, S. C., C. K. Shum, M. Bevis, C. Ji, and C. Y. Kuo, Crustal dilatation observed by GRACE after the 2004 Sumatra-Andaman earthquake, *Science*, **313**, 658–662, 2006.

Hayashi, Y., N. Hamada, T. Kuragano, T. Sakurai, H. Takayama, Y. Hasegawa, and K. Hirata, Detection of the seismic geoid change due to the 2004 Sumatra-Andaman earthquake from satellite altimetry, *Chikyu Monthly*, extra **56**, 32–37, 2006 (in Japanese).

Hirata, K., K. Satake, Y. Tanioka, T. Kuragano, Y. Hasegawa, Y. Hayashi, and N. Hamada, The 2004 Indian Ocean Tsunami: Tsunami source model from satellite altimetry, *Earth Planets Space*, **58**, 195–201, 2006.

Ishii, M., P. M. Shearer, H. Houston, and J. E. Vidale, Extent, duration and speed of the 2004 Sumatra-Andaman earthquake imaged by the Hi-Net array, *Nature*, **435**, 933–936, 2005.

McCloskey, J., S. S. Nalbant, and S. Steacy, Earthquake risk from coseismic stress, *Nature*, **434**, 291, 2005.

National Aeronautics and Space Administration, TOPEX/Poseidon: Ocean Surface Topography Experiment, http://sealevel.jpl.nasa.gov/mission/tp-fact-sheet.pdf, 2001a.

National Aeronautics and Space Administration, Jason-1: An Ocean Odyssey—Ocean Data from Space, http://sealevel.jpl.nasa.gov/mission/jason-1-fact-sheet.pdf, 2001b.

National Earthquake Information Center, U.S. Geological Survey, Preliminary determinations of epicenters weekly listing, ftp://hazards.cr.usgs.gov/weekly/manuscript/, 2005.

Okubo, S., Potential and gravity changes raised by earthquakes and volcanic eruptions—Formulation on the dislocation theory, *J. Geod. Soc. Jpn.*, **40**, 1–16, 1994 (in Japanese with English abstracts).

Sabadini, R., G. Dalla Via, M. Hoogland, and A. Aoudia, A Splash in earth gravity from the 2004 Sumatra earthquake, *EOS Trans. AGU*, **86**, 149, 153, 2005.

Smith, W. H. F. and D. T. Sandwell, Global sea floor topography from satellite altimetry and ship depth soundings, *Science*, **277**, 1956–1962, 1997.

Sun, W. and S. Okubo, Surface potential and gravity changes due to internal dislocations in a spherical earth—II. Application to a finite fault, *Geophys. J. Int.*, **132**, 79–88, 1998.

Wessel, P. and W. H. F. Smith, The Generic Mapping Tools technical reference and cookbook, Version 3.3, 1999.

Y. Hayashi (e-mail: yhayashi@mri-jma.go.jp), K. Hirata, T. Kuragano, T. Sakurai, H. Takayama, Y. Hasegawa, and N. Hamada